High-Frequency Photoelectromagnetic Effect in p-Type InSb

S. C. Choo,* A. M. Etchells, and L. A. K. Watt
Electrical Engineering Department, University of Waterloo, Ontario, Canada
(Received 7 July 1971)

The high-frequency response of the photoelectromagnetic (PEM) effect in p-type InSb has been studied both theoretically and experimentally over the temperature range 77–203 °K. It was found that where the response curves could be characterized by a single time constant, the curves exhibited a high-frequency falloff with a 3-dB/octave slope, in contrast to the 6-dB/octave slope which was characteristic of the photoconductive (PC) response. At temperatures around 200 °K, the same time constant entered into both the PEM and PC response. However, around 77 °K, the PEM time constant was at least 3 orders of magnitude smaller than the PC time constant. This difference was shown theoretically to correspond to the difference between the steady-state electron and hole lifetimes, with which the PEM and PC time constants may, respectively, be identified. The character of the PEM frequency-response curves was found to change as the temperature was increased from 77 °K, with evidence that more than one time constant was involved over the range 104–140 °K. All the response curves observed experimentally can be quantitatively accounted for in terms of a two-independent-level recombination model with parameters which are only slightly different from those previously used by Hollis, Choo, and Heasell.

I. INTRODUCTION

Along with the photoconductivity (PC),[1–3] the photoelectromagnetic (PEM) effect[1,2] has been extensively used to measure bulk-carrier lifetimes in InSb. These measurements have established that in InSb, carrier recombination around room temperature takes place via an interband Auger process, but at lower temperatures indirect recombination through localized levels becomes the dominant process. The recombination centers have been identified[2,3] as donorlike, with energy levels at 0.071 and 0.11 eV above the valence band. In p-type InSb at temperatures below 130 °K when the lower level is operative, the centers exhibit the property of strong minority-carrier trapping.[1,2]

While some of the PC measurements referred to above[3] have been carried out at high light-modulation frequencies, all of the PEM measurements were done under steady-state or low-frequency conditions. It is well known that in the absence of carrier trapping, both the steady-state PEM lifetime $\tau_{PEM}(0)$ and PC lifetime $\tau_{PC}(0)$ are identically equal to the time constant characterizing the transient decay or frequency response of the optically injected carriers; but, when trapping effects occur as in p-type InSb at low temperatures, the relationship between the steady-state lifetimes and transient lifetime becomes much more complex. This is evident from the work of Hollis, Choo, and Heasell[3] (hereafter referred to as HCH) who recently reported measurements of the photoconductive phase-shift lifetime τ_e in p-type InSb from room to liquid-nitrogen temperatures. They found that at low temperatures, τ_e is, in general, frequency dependent, although it is qualitatively similar to $\tau_{PC}(0)$ because their phase-shift measurements were based on the PC response.

The distinction that we have made above between the steady-state and transient lifetimes is of more than academic interest, since InSb detectors operated in both the PC and the PEM mode are in common use in high-speed infrared applications,[4] and while the detectivity of these detectors at low frequencies depends on the steady-state lifetimes, it is the transient lifetimes which determine their speed of response.

It has been shown[5] for the steady-state case that, because the PEM effect is basically a diffusion process, the PEM lifetime is equivalent to the minority-carrier lifetime in extrinsic material. Thus, intuitively one expects that the high-frequency response of the PEM effect would also be governed by the transient lifetime of the minority carriers. Since in p-type InSb at low temperatures, $\tau_{PEM}(0)$ is is typically smaller than $\tau_{PC}(0)$ by several orders of magnitude,[2] a considerable difference may be expected in the frequency response of the PEM and PC effects.

There is, however, a still more fundamental difference to be expected between these two effects, regardless of any trapping effects. As may be seen from Shockley's classical theory of pn junctions,[6] one of the characteristics of minority-carrier diffusive flow is that it exhibits a frequency dependence of the form $(1+\omega^2\tau^2)^{-1/4}$, where τ is the minority-carrier lifetime. The same frequency dependence should therefore also apply to the PEM current, in contrast to the PC current which should vary with ω as $(1+\omega^2\tau^2)^{-1/2}$. To our knowledge, despite the long history of the PEM effect, such a frequency dependence has never been observed experimentally

in any of the well-known semiconductors.

In this connection, InSb is a particularly convenient material for study, since for this material, a very simple situation obtains at temperatures $\gtrsim 200\,^{\circ}\mathrm{K}$, owing to the absence of trapping effects. The fact that a common lifetime enters into both the PEM and PC effects suggests that, provided surface effects are eliminated, the frequency response of these two effects should show the same break frequency, with a 6-dB/octave rate of falloff at $\omega \gg 1/\tau$ for the PC effect, but only 3 dB/octave for the PEM effect.

The above considerations suggest that it would be of interest to investigate the high-frequency PEM effect in p-type InSb from near room temperature to liquid-nitrogen temperature, and compare it to the high-frequency PC effect. While there exist a few reports[7-9] on the measurement of the PEM response time in InSb, these are isolated measurements done on PEM detector elements at room temperature. The work to be described in this paper is believed to be the first systematic investigation of the high-frequency PEM effect in InSb. A theory will be presented which describes the high-frequency PEM effect in the presence of carrier trapping, and which quantitatively accounts for the data obtained from 203 to 77 °K.

II. EXPERIMENTAL PROCEDURE

The apparatus used to measure the PEM and PC response consists of three main parts: (a) a light source, (b) a detection system, and (c) a temperature control and magnet system.

A. Light Source

The light source is a Monsanto M120C GaAs light emitting diode which emits radiation at 0.9 μ with a linewidth of about 0.1 μ. According to the manufacturer's specifications, the emission turn "on" and turn "off" time is 1 nsec giving the diode a modulation bandwidth of approximately 100 MHz. In our experiment, the diode was sinusoidally modulated from 1 KHz to 40 MHz around a dc bias chosen to ensure that the waveform of the light output signal is sinusoidal with negligible distortion. For the frequency response measurements, it was necessary to maintain a constant light output at all frequencies. This was done by monitoring the light output using an HP5082-4205 high-frequency photodiode detector, biased to have a cutoff frequency of >100 MHz.

B. Detection System

The electrical output signal from the InSb sample was fed to a Hewlett Packard HP3500A amplifier terminated in 50 Ω and then to a Bruel and Kjaer tuned rf voltmeter and probe. Measurements below 100 KHz were made using a Princeton Applied Research lock-in amplifier.

Particular care was taken to check the system for uniformity of frequency response and for voltage linearity at a given frequency, and where deviations occurred, the required corrections were made. With this system, the minimum detectable signal is 2×10^{-7} V across a 50-Ω resistor.

C. Temperature Control and Magnet System

An Andonian Associates type IV-4-0500 Dewar was used to house the sample. It is a standard gas-exchange Dewar with a detachable tail section and nitrogen shield. The outer tail section has Pyrex window ports to the sample mounting platform. A resistance heater is provided at the base of the sample mount for temperature control. The sample temperature was monitored by a copper-constantan thermocouple placed adjacent to the sample on its mounting block. With this system, the temperature could be maintained at $\pm 0.5\,^{\circ}\mathrm{C}$ for periods of up to $\frac{1}{2}$ h, over the range 77–250 °K.

A Spectro-Magnetic model 6021 electromagnet was used to provide fields from 40 to 8000 G. The magnet has adjustable pole pieces between which the Dewar tail containing the sample could be inserted. The pole pieces were large enough that a Hall probe could be inserted directly behind the Dewar tail and in line with the sample mounting position. The magnetic field was measured with a Bell 110A gaussmeter with an accuracy of ± 3% of the reading.

The samples used were all p-type InSb and were cut from a zinc-doped single-crystal ingot supplied by Cominco. They were in the form of thin strips approximately 7 mm long, 3 mm wide, and 3×10^{-1} mm thick in the case of Hall specimens, but between 10^{-1} to 5×10^{-1} mm thick in the case of PEM or PC specimens. Contacts to the specimens were made using In + 5% Ag solder. To obtain surfaces with low surface-recombination velocity, the specimens were electropolished in an electrolyte of 1% HNO_3 in ethylene glycol.[3,10]

III. THEORY OF HIGH-FREQUENCY PEM AND PC EFFECTS

The theory is most conveniently divided into two sections. The first section will deal with carrier transport without explicit reference to a specific recombination model. The effect of recombination will be expressed through a frequency-dependent lifetime parameter, one for electrons and one for holes, in analogy to the steady-state lifetime parameters used by Zitter.[5] In the next section, expressions will be derived for these lifetime parameters in terms of a specific recombination model.

We consider a slab-shaped semiconductor sample with thickness d in the y direction, placed in a magnetic field of flux density B in the z direction. Light of intensity $Ie^{j\omega t}$ falls on one surface, as

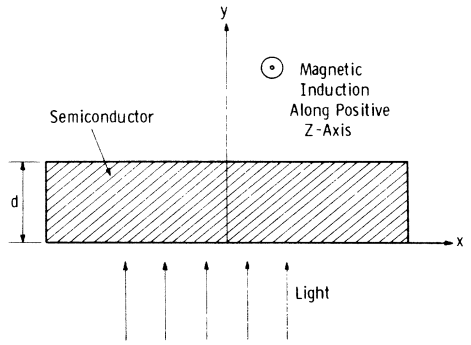

FIG. 1. Sample orientation for the PEM effect.

shown in Fig. 1. It is assumed that (i) small-signal approximations are valid, (ii) the light is absorbed entirely at the illuminated surface and not in the bulk, (iii) the sample is sufficiently long and wide that edge effects can be ignored, (iv) the surface recombination velocities of both surfaces are negligible and the effect of a surface space-charge layer can be neglected, and (v) the radian frequency ω of light modulation is low compared to the reciprocal of the dielectric relaxation time, so that space-charge relaxation effects[11] can be ignored.

The carrier-transport equations, including the effect of the magnetic field, are given by

$$\vec{J}_n = qD\,\nabla(\Delta n) - \mu\vec{J}_n\times\vec{B} + q\mu(n+\Delta n)\vec{E}\,, \tag{1}$$

$$b\vec{J}_p = -qD\,\nabla(\Delta p) + \mu\vec{J}_p\times\vec{B} + q\mu(p+\Delta p)\vec{E}\,, \tag{2}$$

where $\vec{J}_n$ and $\vec{J}_p$ are the electron and hole current densities, q the electronic charge, n and p the equilibrium electron and hole concentrations, Δn and Δp the corresponding excess concentrations, μ the electron mobility, D the electron-diffusion constant, b the electron-to-hole mobility ratio, and $\vec{E}$ the electric field.

Total-current continuity is expressed by

$$\nabla\cdot(\vec{J}_n+\vec{J}_p) = 0\,, \tag{3}$$

where the displacement current has been ignored due to assumption (v). For ac excitation, the continuity equations for the individual electron and hole currents are given by

$$j\omega\Delta n = -R_n + q^{-1}\nabla\cdot\vec{J}_n\,, \tag{4}$$

$$j\omega\Delta p = -R_p - q^{-1}\nabla\cdot\vec{J}_p\,, \tag{5}$$

where R_n and R_p are, respectively, the net recombination rate for electrons and holes.

We now introduce two lifetime parameters $\tau_n(j\omega)$ and $\tau_p(j\omega)$ as follows:

$$\Delta n/\tau_n(j\omega) \triangleq j\omega\Delta n + R_n \tag{6}$$

and

$$\Delta\rho/\tau_p(j\omega) \triangleq j\omega\Delta p + R_p\,. \tag{7}$$

$\tau_n(j\omega)$ and $\tau_p(j\omega)$ are therefore effective frequency-dependent lifetimes, whose functional dependence on $j\omega$ depends on the particular recombination model chosen. In the steady state, they reduce to the same lifetime parameters as used by Zitter.

Rewriting Eqs. (4) and (5) and using Eq. (3), we find

$$\nabla\cdot\vec{J}_n = -\nabla\cdot\vec{J}_p = q\Delta n/\tau_n(j\omega) = q\Delta p/\tau_p(j\omega)\,. \tag{8}$$

Since the system of equations, (1), (2), and (8) is formally the same as that employed by Zitter, we may carry over his solution with a slight modification to take into account the finite thickness of the sample. The result, for the PEM short-circuit current per unit sample width, i_{PEM}, is as follows:

$$i_{\mathrm{PEM}} = (1+1/b)q\eta\mu BL_D^* FIe^{j\omega t}\,, \tag{9}$$

where η is the quantum efficiency,

$$(L_D^*)^2 = \frac{(1+c)D\tau_{\mathrm{PEM}}(j\omega)}{1+\mu^2B^2+bc(1+\mu^2B^2/b^2)}\,, \tag{10}$$

$$\tau_{\mathrm{PEM}} = \frac{\tau_n(j\omega)+c\tau_p(j\omega)}{1+c}\,, \tag{11}$$

and

$$c = n/p\,. \tag{12}$$

The factor F is the ratio of the actual PEM current to the ideal PEM current which would be obtained for a thick sample with $d \gg L_D^*$. It is given by

$$F = \tanh(d/2L_D^*)\,. \tag{13}$$

For the photoconductive short-circuit current per unit sample width, i_{PC}, the result is

$$i_{\mathrm{PC}} = (1+1/b)\eta\mu E_x\tau_{\mathrm{PC}}(j\omega)Ie^{j\omega t}\,, \tag{14}$$

where

$$\tau_{\mathrm{PC}}(j\omega) = \frac{\tau_n(j\omega)+\tau_p(j\omega)/b}{1+1/b}\,. \tag{15}$$

In the low-frequency limit, $\omega\to 0$, Eqs. (9)–(15) are, of course, identical to Zitter's results.

Recombination Model

In previous interpretation of steady-state PEM-PC lifetime data in InSb, Laff and Fan[2] have used a two-interacting-level model, consisting of a set of divalent flaws. However, HCH[3] have found that their Hall effect and photoconductive phase-shift lifetime data are more consistent with a two-independent-level model consisting of two sets of single-level flaws, than the interacting-level model.

In the present work, we have also found that a two-independent-level model can satisfactorily account for our Hall and PEM high-frequency data, and in what follows we shall therefore develop expressions for $\tau_n(j\omega)$ and $\tau_p(j\omega)$ in terms of such a

model.

We suppose that there are two sets of flaws, of concentrations N_1 and N_2, lying at energies E_1 and E_2, respectively, in the band gap. Each flaw of type j ($j=1, 2$) is characterized by a hole-capture coefficient c_{pj}, and an electron-capture coefficient c_{nj}. If we denote the equilibrium concentration of filled and empty flaws by N_j^- and N_j^+ ($=N_j - N_j^-$), respectively, we have the ratio $N_j^+/N_j^- = \gamma e^{(E_j-\xi)/kT}$, where ξ is the Fermi level, γ the degeneracy factor, k Boltzmann's constant, and T the absolute temperature. Previous lifetime studies[2,3] have indicated that the flaws are donorlike. We shall therefore assume that $\gamma = \frac{1}{2}$.

By considering the interaction of the flaws with the valence and conduction bands, and using n_j and p_j to denote the equilibrium carrier concentrations when the Fermi level coincides with E_j, we may readily write down the continuity equations for the electron and hole currents as follows[12]:

$$\frac{\partial \Delta n}{\partial t} = -\sum_j R_{nj} + q^{-1}\nabla \cdot \vec{J}_n \,, \tag{16}$$

$$\frac{\partial \Delta p}{\partial t} = -\sum_j R_{pj} - q^{-1}\nabla \cdot \vec{J}_p \,, \tag{17}$$

$$\frac{\partial \Delta N_j^-}{\partial t} = R_{nj} - R_{pj} \quad (j=1, 2) \,, \tag{18}$$

where

$$R_{nj} = c_{nj}\left[(n+\Delta n)(N_j^+ - \Delta N_j^-) - n_j(N_j^- + \Delta N_j^-)\right] \tag{19}$$

and

$$R_{pj} = c_{pj}\left[(p+\Delta p)(N_j^- + \Delta N_j^-) - p_j(N_j^+ - \Delta N_j^-)\right] . \tag{20}$$

Finally, charge neutrality constraint provides the relation

$$\Delta n + \Delta N_1^- + \Delta N_2^- = \Delta p \,. \tag{21}$$

The small-signal expansion of Eqs. (16)–(20), along with Eq. (21), leads to the following matrix equation:

$$\begin{bmatrix} D+a_{11} & a_{12} & a_{13} \\ a_{21} & D+a_{22} & a_{23} \\ a_{31} & a_{32} & D+a_{33} \end{bmatrix} \times \begin{bmatrix} \Delta n \\ \Delta p \\ \Delta N_2^- \end{bmatrix} = \begin{bmatrix} q^{-1}\nabla \cdot \vec{J}_n \\ -q^{-1}\nabla \cdot \vec{J}_p \\ 0 \end{bmatrix} , \tag{22}$$

where D is the operator $\partial/\partial t$ and the a_{ij}'s are functions of the equilibrium statistics and the capture coefficients, as given in the Appendix.

For ac excitation, $D = j\omega$, and solving for Δn and Δp, we find

$$\Delta n/\tau_n(j\omega) = q^{-1}\nabla \cdot \vec{J}_n \,, \tag{23}$$

$$-\Delta p/\tau_p(j\omega) = q^{-1}\nabla \cdot \vec{J}_p \,, \tag{24}$$

where

$$|\tau_n(j\omega)| = \tau_n(0)\sum_{i=1}^{3} \frac{A_i(n)}{(1+\omega^2\tau_i^2)^{1/2}} \tag{25}$$

and

$$|\tau_p(j\omega)| = \tau_p(0)\sum_{i=1}^{3} \frac{A_i(p)}{(1+\omega^2\tau_i^2)^{1/2}} \,. \tag{26}$$

The amplitude coefficients must satisfy the conditions

$$\sum A_i(n) = \sum A_i(p) = 1 \,, \tag{27}$$

since in the limiting case of zero frequency, $\tau_n(\omega) \to \tau_n(0)$ and $\tau_p(\omega) \to \tau_p(0)$. These coefficients are given by

$$A_1(n, p) = \frac{\tau_1^2 - \tau_1\tau_a(n, p) + \tau_a(n, p)\tau_b(n, p)}{(\tau_1-\tau_2)(\tau_1-\tau_3)} \,, \tag{28}$$

$$A_2(n, p) = \frac{\tau_2^2 - \tau_2\tau_a(n, p) + \tau_a(n, p)\tau_b(n, p)}{(\tau_2-\tau_1)(\tau_2-\tau_3)} \,, \tag{29}$$

$$A_3(n, p) = \frac{\tau_3^2 - \tau_3\tau_a(n, p) + \tau_a(n, p)\tau_b(n, p)}{(\tau_3-\tau_1)(\tau_3-\tau_2)} \,, \tag{30}$$

with

$$\tau_a(n) = \left[\sum H_i^{-1}(1+u_{pj})\right]/(1+\sum u_{pj}) \quad (i \neq j; \quad i, j = 1, 2) \,, \tag{31}$$

$$\tau_b(n) = \left[\sum H_j(1+u_{pj})\right]^{-1} \,, \tag{32}$$

$$\tau_a(p) = \left[\sum H_i^{-1}(1+u_{nj})\right]/(1+\sum u_{nj}) \,, \tag{33}$$

$$\tau_b(p) = \left[\sum H_j(1+u_{nj})\right]^{-1} \,, \tag{34}$$

$$u_{pj} = c_{pj}N_j^-/H_j \,, \tag{35}$$

$$u_{nj} = c_{nj}N_j^+/H_j \,, \tag{36}$$

$$H_j = c_{nj}(n+n_j) + c_{pj}(p+p_j) \,. \tag{37}$$

In Eqs. (25) and (26), $\tau_n(0)$ and $\tau_p(0)$ are the steady-state lifetimes, and are given by[12]

$$\tau_n(0) = (1+\textstyle\sum_j u_{pj})/(\sum_j \tau_{jd}^{-1}), \tag{38}$$

$$\tau_p(0) = (1+\textstyle\sum_j u_{nj})/(\sum_j \tau_{jd}^{-1}) \quad (j=1, 2) \,, \tag{39}$$

where

$$\tau_{jd}^{-1} = c_{nj}c_{pj}N_j(n+p+\textstyle\sum_j N_j^+N_j^-/N_j)/H_j \,. \tag{40}$$

τ_1, τ_2, and τ_3 are the time constants of the system given by the negative inverse of the roots of the characteristic equation for the system matrix

$$D^3 + \alpha_2 D^2 + \alpha_1 D + \alpha_0 = 0 \,, \tag{41}$$

where

$$\alpha_0 = (a_{11}a_{23}a_{33} + a_{12}a_{23}a_{31} + a_{13}a_{21}a_{32}) - (a_{11}a_{23}a_{32} + a_{12}a_{21}a_{33} + a_{13}a_{22}a_{31}) \,,$$

$$\alpha_1 = (a_{11}a_{22} + a_{22}a_{33} + a_{11}a_{33}) - (a_{12}a_{21} + a_{23}a_{32} + a_{13}a_{31}) \,,$$

$$\alpha_2 = a_{11} + a_{22} + a_{33} .$$

In the analysis of our data, exact solutions for the three time constants were obtained numerically. However, we have found that in all the situations of interest, either one or two of the time constants are dominant. In this case, convenient analytical approximations are available.[12]

Thus, when two of the time constants are longer than the third (i.e., τ_1, $\tau_2 \gg \tau_3$), they are given approximately by[12]

$$\tau_{1,2} \approx (\alpha_1/2\alpha_0) \pm [(\alpha_1/2\alpha_0)^2 - (\alpha_2/\alpha_0)]^{1/2} , \quad (42)$$

with

$$\tau_3 \approx 1/\alpha_2 . \quad (43)$$

If, in addition, $\tau_1 \gg \tau_2$, so that τ_1 is the dominant time constant, further simplification follows:

$$\tau_1 \approx \alpha_1/\alpha_0 , \quad (44)$$

$$\tau_2 \approx \alpha_2/\alpha_1 , \quad (45)$$

$$\tau_3 \approx 1/\alpha_2 . \quad (46)$$

After some algebraic manipulation, the following expressions for the right-hand sides of Eqs. (44)–(46) are obtained[12]:

$$\frac{\alpha_1}{\alpha_0} = \sum \tau_{jd}^{-1} / (1 + \sum g_j) , \quad (47)$$

$$\frac{\alpha_2}{\alpha_1} = \frac{\sum (1 + u_{ni} + u_{pi})}{H_i} \Big/ (1 + \sum g_j) \quad (i \neq j; \quad i, j = 1, 2) , \quad (48)$$

$$1/\alpha_2 = 1/\sum H_j (1 + u_{nj} + u_{pj}) , \quad (49)$$

where

$$g_j = u_{nj}(1 + u_{pj}) + u_{pj} + (\tau_j H_i)^{-1}, \quad (50)$$

$$\tau_j^{-1} = c_{nj} c_{pj} N_j \frac{n + p + N_j^- N_j^+}{N_j} \Big/ H_j . \quad (51)$$

IV. SIMPLIFIED SOLUTIONS FOR PEM AND PC EFFECTS

The complete system of equations describing the frequency dependence of the PEM and PC effects of a two-level model is given by Eqs. (11), (15), (25)–(41), and (42)–(51). We now wish to show that this system of equations simplifies considerably when applied to p-type InSb at around 200 and 77 °K, and that it predicts the difference in high-frequency behavior between the PEM and PC effects at these temperatures, as anticipated in Sec. I. To do so, we assume a p-type sample with a hole concentration of about 10^{14} cm^{-3} at 77 °K, and, as an estimate, we use parameter values for the two-independent-level model given by HCH: $c_{n1} = 3 \times 10^{-5}$, $c_{p1} = 6 \times 10^{-10}$, $c_{n2} = 2 \times 10^{-6}$, $c_{p2} = 2 \times 10^{-8}$ cm^3 sec^{-1}; $E_1 - E_v = 0.071$ eV, $E_2 - E_v = 0.11$ eV; $N_1, N_2 \approx 10^{14}$ cm^{-3}.

A. 200 °K

The situation is particularly simple around this temperature with the Fermi level close to level 2 but far above level 1. From the parameter values we have assumed, it is easily shown that u_{n1}, u_{n2}, u_{p1}, $u_{p2} \ll 1$, which is consistent with the absence of carrier-trapping effects established in previous work for these temperatures.[1-3] Inspection of Eqs. (25)–(34) then shows that $\tau_n(j\omega) = \tau_p(j\omega)$, i.e., both the electrons and holes have identical frequency response.

Using Eqs. (38) and (39) to calculate the steady-state lifetimes and Eqs. (44)–(46) to evaluate the three time constants, we find that

$$\tau_1 = \tau_p(0) = \tau_n(0) = \tau_{1d} \approx (c_{p2} N_2)^{-1} [(n + n_2)/(p + p_2)] , \quad (52)$$

$$\tau_2 \approx 1/H_2 , \quad (53)$$

$$\tau_3 \approx 1/H_1 . \quad (54)$$

We shall now establish that τ_1 is the dominant time constant in both the PEM and PC response by first observing from Eqs. (31)–(34) that $\tau_a(n, p) \approx \tau_2$ and $\tau_b(n, p) \approx \tau_3$, and since $\tau_1 \gg \tau_2 \gg \tau_3$, Eq. (28) gives $A_1(n, p) \approx 1$. By Eq. (27), this implies that $A_1(n, p)$ is the largest of the three amplitude coefficients. Hence

$$\tau_p(\omega) = \tau_n(\omega) = \tau/(1 + \omega^2\tau^2)^{1/2} , \quad (55)$$

where $\tau = \tau_1 = \tau_p(0) = \tau_n(0)$.

To obtain the frequency response of the PEM and PC effects, we substitute the above expression for $\tau_p(\omega)$ and $\tau_n(\omega)$ in Eqs. (11) and (15), with the result that, for a thick sample with $d \gg L_D^*$,

$$i_{\mathrm{PEM}} \propto 1/(1 + \omega^2\tau^2)^{1/4} , \quad (56)$$

$$i_{\mathrm{PC}} \propto 1/(1 + \omega^2\tau^2)^{1/2} . \quad (57)$$

The above equations show that the same lifetime parameter enters into both the PEM and PC response, as one expects in the absence of trapping. However, the rate of falloff of the PEM response for $\omega \gg (1/\tau)$ is 3 dB/octave, which is half of that of the PC response. This difference is a consequence of the fact that, as shown by Eqs. (9) and (10), the PEM response is directly proportional to the diffusion length, rather than to the lifetime as is the case with the PC response.

B. 77 °K

Around this temperature with the Fermi level close to level 1 but well below level 2, the following inequalities apply: $\tau_{1d} \gg \tau_{2d}$; u_{p1}, $u_{p2} \ll 1$; and $u_{n1} \gg u_{n2}$, 1. The last inequality is indicative of strong electron trapping at level 1.

With the above simplifications, we find from Eqs. (44)–(49) that the largest and the smallest time constants are, respectively, equal to the steady-state lifetime for holes and for electrons. Thus,

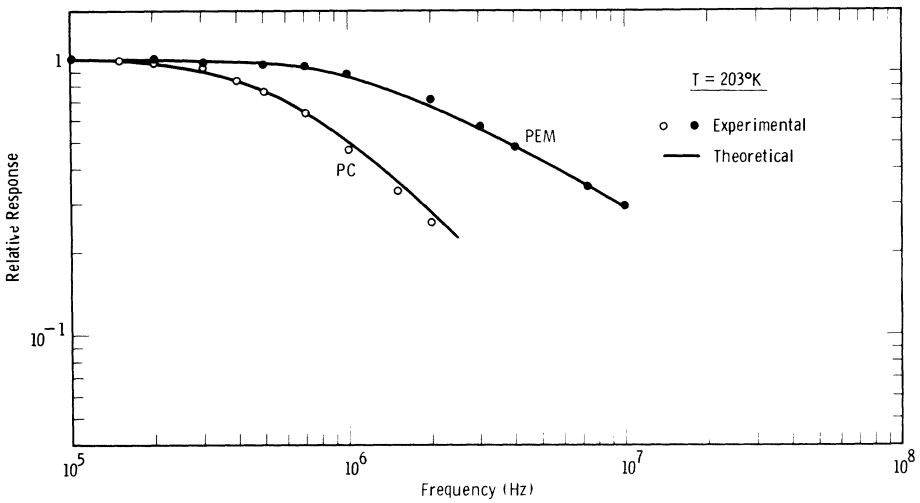

FIG. 2. Comparison of PC and PEM frequency response at 203 °K for a sample of thickness 9×10^{-3} cm. The magnetic-flux density used was 0.2 Wb/m^2. The theoretical PEM response was calculated from Eqs. (9)–(13).

$$\tau_1 = \tau_p(0) \approx 1/H_1 \approx 1/c_{p1}(p+p_1)\,, \tag{58}$$

$$\tau_3 = \tau_n(0) \approx \tau_{1d} \approx 1/c_{n1}N_1^+\,, \tag{59}$$

with

$$\tau_2 \approx 1/H_2 \approx 1/c_{p2}(p+p_2)\,. \tag{60}$$

It will now be shown that while τ_1 dominates the PC response, it is τ_3 which governs the PEM response. This can be done simply by showing that $A_1(p)\approx 1$ and $A_3(n)\approx 1$. To evaluate these coefficients, we refer to Eqs. (31)–(34) and obtain the following results: $\tau_a(n)=1/H_2$, $\tau_b(n)=1/H_1$; $\tau_a(p)=\tau_2$, $\tau_b(p)=\tau_3$. Comparison of these expressions with Eqs. (58) and (60) shows that $\tau_a(n)\tau_b(n)=\tau_1\tau_2$, and since τ_1 is the largest time constant, Eq. (28) gives $A_1(p)\approx 1$. In the same way, it can be shown that $A_3(n)\approx_1$.

The final result for the PEM and PC response is then

$$i_{\rm PEM} \propto \tau_n(0)/[1+\omega^2\tau_n(0)^2]^{1/4} \tag{61}$$

and

$$i_{\rm PC} \propto \tau_p(0)/[1+\omega^2\tau_p(0)^2]^{1/2}\,. \tag{62}$$

The above relations state that when strong minority-carrier trapping occurs, the frequency response of the PEM and PC effects is governed, in each case, by a single time constant. In the case of the PEM effect, this time constant is equivalent to the steady-state minority carrier lifetime; but, in the case of the PC effect, it is the same as the longer steady-state majority carrier lifetime.

From Eqs. (58) and (59) and the assumed parameter values, $\tau_p(0)$ and $\tau_n(0)$ were found to be on the order of 10^{-6} and 10^{-10} sec, respectively. One may therefore reasonably expect the response time of the PEM effect to be some 3 to 4 orders of magnitude smaller than that of the PC effect.

V. EVALUATION OF EXPERIMENTAL RESULTS AND DISCUSSION

A. Comparison of PEM and PC Frequency-Response Measurements

1. *High Temperatures*

In early experiments carried out at temperatures around 200 °K it was found that, contrary to the predictions of Eqs. (56) and (57), the PEM frequency response consistently gave a higher break frequency than the PC response. A typical set of measurements showing this effect at 203 °K is given in Fig. 2. The discrepancy was clearly too large to be accounted for by experimental error, and could not be resolved until it was recognized that in attempting to increase the output signal from the sample, the thickness of the sample might have been so far reduced that it was no longer large compared to the ambipolar diffusion length. To test this hypothesis, we assumed that the PC break frequency gave the true bulk lifetime, since the PC response is independent of sample thickness as long as surface recombination effects are negligibly small. Then, using this value of lifetime (2.6×10^{-7} sec) and the magnetic field of 0.2 Wb/m^2 used in the experiment, along with values of electron and hole mobilities taken from HCH as estimates, we calculated L_D^*, and obtained a ratio (d/L_D^*) of 1.2, suggesting that the thick-sample approximation used in Eqs. (56) and (57) might not be applicable in the present case. As a further test, the theoretical PEM response was computed by including the factor F defined by Eq. (13) in Eq. (56) and using the above value of (d/L_D^*) in calculating F. The results of the computation, along with those for the PC response calculated from Eq. (57), are shown as solid lines in Fig. 2, and, as can be seen, the agreement with the experimental data is excellent. In all subsequent experiments, the sample dimen-

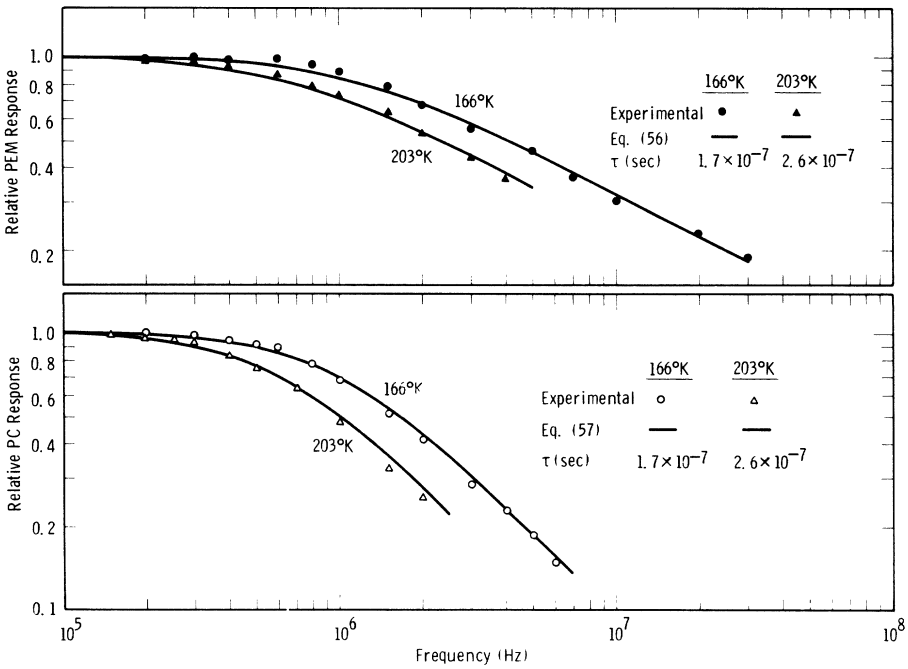

FIG. 3. Comparison between PC and PEM frequency response at 203 and 166 °K for a thick sample. At each temperature, the same time constant was used in calculating both the theoretical PC and PEM response. The magnetic-flux density used was 0.1 Wb/m^2.

sions were always made such that the thick-sample approximation can be justified.

Examples of high-frequency measurements of the PEM and PC effects for such a thick sample are shown in Fig. 3 for 203 and 165 °K. The solid curves were obtained from Eqs. (56) and (57), with $\tau = 2.6\times10^{-7}$ sec for 203 °K and 1.7×10^{-7} sec for 165 °K. Their close fit with the experimental data serves to confirm the general validity of these equations in situations where both the PEM and PC effects are characterized by the same lifetime.

2. *Low Temperatures*

According to the theoretical considerations in Sec. IV B [Eqs. (61) and (62)], cooling the p-type sample down to liquid-nitrogen temperatures should produce a drastic difference between the PEM frequency response and the PC response. These predictions are largely borne out by the measurements shown in Fig. 4 for 80 °K. The PC response can be described by Eq. (62) with a time constant of 6.9×10^{-6} sec. The PEM response, on the other hand, remains essentially flat up to 40 MHz, the upper limit of our measurement range, indicating that the response time must be smaller than 2×10^{-9} sec.

B. PEM Frequency-Response Measurements from 77 to 203 °K

Aside from the relatively simple situations at high and low temperatures as discussed above, the

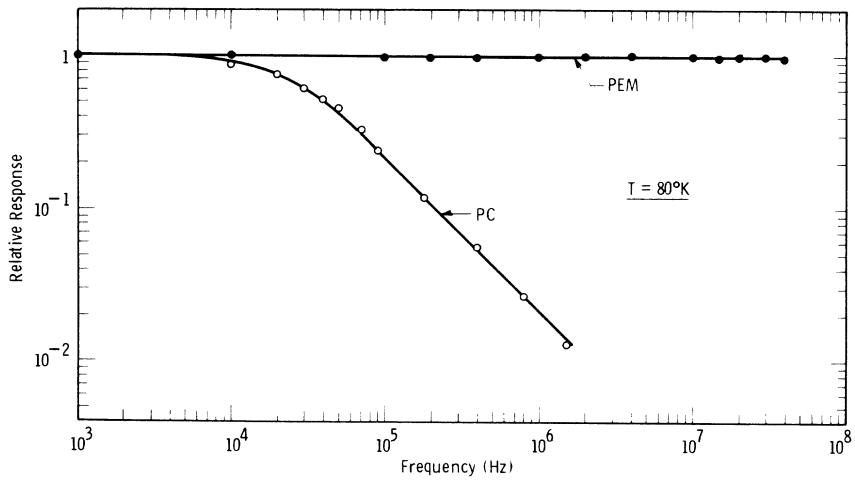

FIG. 4. Comparison of PC and PEM frequency response at 80 °K for a p-type sample. The magnetic-flux density used was 0.1 Wb/m^2.

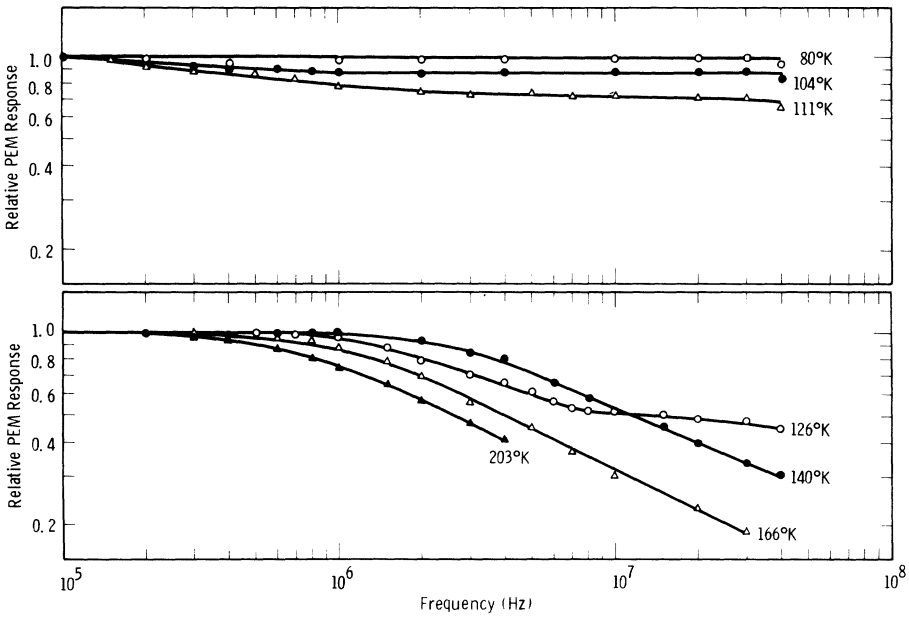

FIG. 5. Comparison of PEM frequency response for a p-type sample at different temperatures.

general behavior of the high-frequency PEM effect is quite complex. Figure 5 shows the change in the character of the frequency response as the temperature is varied from 77 to 203 °K. In particular, we find that more than a single time constant is involved over the range 104–140 °K.

In order to explain the data over the complete temperature range, we have employed a two-independent-level model as previously described, making use of Eqs. (25)–(37) along with Eqs. (9)–(12). In all cases considered, exact solutions for the three time constants τ_1, τ_2, and τ_3 were obtained numerically. The values of the recombination parameters used are shown below in Table I—the values of the energy levels were assumed to be identical to those used in HCH; the remaining parameters, however, were chosen to fit both the PEM and Hall data (not shown) obtained for this particular sample. The Hall data in the extrinsic range were used to provide an initial estimate for the trap concentrations N_1 and N_2, by following the same procedure as in HCH. Then, by an iterative process, adjustments were made in the values of the capture coefficients and trap concentrations until optimum fits were achieved simultaneously for both the PEM and Hall data. The solid curves in Figs. 6–9 are typical examples of the optimum fits obtained for the PEM data over the complete temperature range investigated, and, as can be seen, the agreement is, in all cases, better than 10%. Note that where more than one time constant is required to explain the data, the figure also shows the individual components associated with each of the time constants.

In order to see more clearly the relationship between the calculated values of τ_1, τ_2, and τ_3 as well as its changes as the temperature is varied, we have plotted these time constants as a function of temperature in Fig. 10. For comparison, we have also included plots of the steady-state lifetimes $\tau_n(0)$ and $\tau_p(0)$. The circles in the figure denote the values of the dominant time constants used in fitting the experimental PEM data; conversely, they may be regarded as values extracted from the data. Those circles which are filled correspond to cases where the time constants are well resolved since, within the frequency range of measurements, a significant falloff of the particular components involved has taken place. The half-filled circles are those partially resolved cases where only some falloff has occurred, and, finally, the unfilled circles are for the unresolved cases where there has been no falloff at all.

A point of interest in Fig. 10 is the close correspondence between τ_1 and $\tau_p(0)$ throughout the temperature range considered. A similar correspondence exists between τ_3 and $\tau_n(0)$ but only at the low-temperature end. In an earlier section,

TABLE I. Parameters of two-independent-level model used to fit PEM and Hall data, along with a net shallow-acceptor concentration of 3×10^{14} cm^{-3}.

	$j=1$	$j=2$
$E_j - E_v$ (eV)	0.071	0.11
c_{pj} (cm^3 sec^{-1})	6×10^{-10}	2×10^{-8}
c_{nj} (cm^3 sec^{-1})	1×10^{-4}	7×10^{-7}
N_j (cm^{-3})	4×10^{13}	1.3×10^{14}

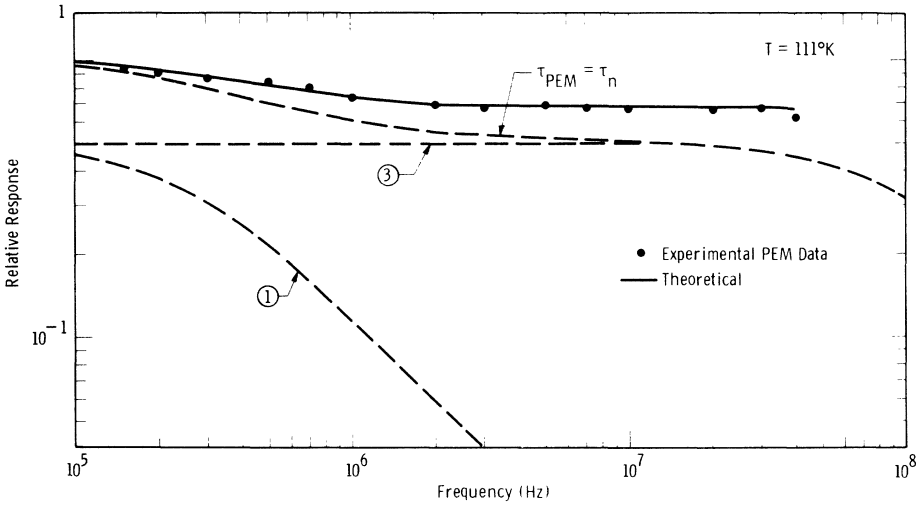

FIG. 6. Comparison between theoretical and experimental PEM frequency response for the p-type sample of Fig. 5 at 111 °K. The theoretical curve was computed by using recombination parameter values given in Table I. The dashed lines show the resolution of the theoretical response into first $\tau_{PEM}(=\tau_n)$ from Eq. (11), and then the components which make up τ_n [Eq. (25)]. Curves 1 and 3 are the components associated with τ_1 and τ_3, respectively.

we have shown by means of a simplified analysis how to establish the correspondence between $\tau_p(0)$ and τ_1 at 200 and 77 °K, and between $\tau_n(0)$ and τ_3 at 77 °K. A similar analysis can be applied to show that $\tau_p(0) \approx \tau_1$ throughout the temperature range. However, our principal concern for the present is with the time constants themselves. In what follows, we shall carry out a simple analysis of the behavior of the time constants as a function of temperature, since aside from the physical insight it would provide, such an analysis would allow us to assess the sensitivity of the fit of the data to the values of the recombination parameters chosen for our computations.

C. Simple Analysis of Time Constants

In carrying out the analysis, we refer to the approximate solutions for the time constants given by Eqs. (44)–(46), under the assumption that the three time constants are well separated. Although it is clear from Fig. 10 that at some of the intermediate temperatures τ_1 and τ_2 are fairly close together, we have found that even in these cases, Eqs. (44) and (45) provide an adequate description of the temperature dependence of these time constants.

1. *Time Constant* τ_1

The behavior of τ_1 over the complete temperature range can be described by a simplified form of Eq. (47):

$$\tau_1^{-1} = (\tau_{1d}^{-1} + \tau_{2d}^{-1})/(1 + u_{n1} + u_{n2}) \ . \tag{63}$$

At the low-temperature end, (77–100) °K, $\tau_{1d} \ll \tau_{2d}$ and $u_{n1} \gg u_{n2}$, 1, so that $\tau_1 \approx u_{n1}\tau_{1d} \approx 1/c_{p1}(p + p_1)$, which is the same result obtained in Eq. (58) by using slightly different values of the recombination parameters. The decrease of τ_1 with increasing temperature in this temperature range is attributed to the decrease in u_{n1} corresponding to the increase

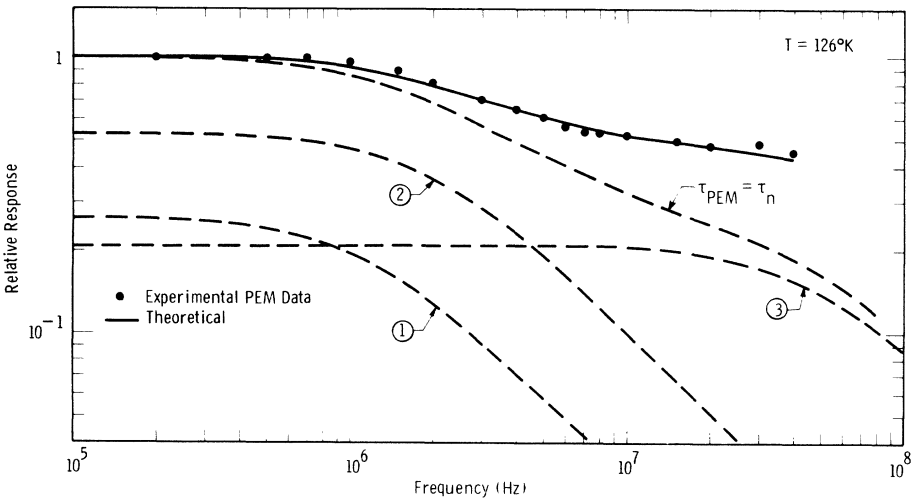

FIG. 7. Comparison between theoretical and experimental PEM frequency response for the p-type sample of Fig. 5 at 126 °K. The theoretical curve was computed by using recombination parameter values given in Table I. The dashed lines show the resolution of the theoretical response into first τ_{PEM} $(=\tau_n)$ from Eq. (11), and then the components which make up τ_n [Eq. (25)]. Curves 1, 2, and 3 are the components associated with τ_1, τ_2, and τ_3, respectively.

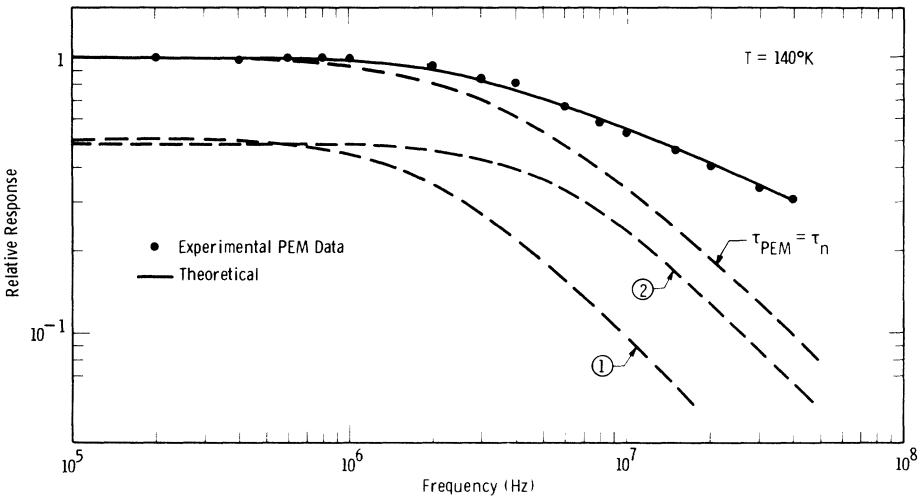

FIG. 8. Comparison between theoretical and experimental PEM frequency response for the p-type sample for Fig. 5 at 140 °K. The theoretical curve was computed by using recombination parameter values given in Table I. The dashed lines show the resolution of the theoretical response τ_{PEM} into first τ_{PEM} ($=\tau_n$) from Eq. (11), and then the components which make up τ_n [Eq. (25)]. Curves 1 and 2 are the components associated with τ_1 and τ_2, respectively.

in p_1 as the Fermi level moves up the band gap, away from level 1.

As we raise the temperature, τ_{1d} and τ_{2d} become comparable, but still with $\tau_{1d} < \tau_{2d}$. At the same time, u_{n1} starts to decrease. Thus, around 111 °K although level 1 still remains the dominant level, level 2 is beginning to exert its effect.

With further increase in temperature, $u_{n1} < u_{n2}$ and $H_1 > H_2$, and level 2 takes over. At first $\tau_1 \approx (1+u_{n2})\tau_{2d}$, but eventually $\tau_1 \approx \tau_{2d}$. The increase of τ_1 from 150 to 190 °K corresponds to the increase of τ_{2d} mainly through n, since over this temperature range the increase in n eventually causes the following inequalities to apply in Eq. (40) for τ_{2d}: $c_{n2}(n+n_2) > c_{p2}(p+p_2)$ and $n > n_2$, while $p > n > \sum(N_j^- N_j^+/N_j)$.

From the above analysis, it is clear that the dip in the τ_1 curve is the result of two opposing tendencies: the decrease of τ_1 due to u_{n1} through p_1, against its increase due to τ_{2d} through n.

2. *Time Constant* τ_2

From 77 to 111 °K, when u_{n1} is very large, Eq. (48) reduces to the following simple form:

$$\tau_2 = 1/H_2 \ .$$

Precisely the same solution applies at temperatures higher than 150 °K, but for a different reason, viz., u_{n1}, $u_{n2} \ll 1$ and $H_1 \gg H_2$.

At the intermediate temperatures 111–150 °K, u_{n2} is comparable to u_{n1}, and

$$\tau_2^{-1} \approx H_2 \left(1 + \frac{u_{n2}}{1+u_{n1}}\right) \approx c_{p2}(p+p_2) + \frac{c_{n2}N_2}{1+u_{n1}} \frac{p}{p+p_2} \ . \tag{64}$$

The main contribution to the temperature dependence of τ_2 over the complete temperature range is therefore due to H_2. At the low temperatures (77–111 °K), τ_2 is a slowly decreasing function of

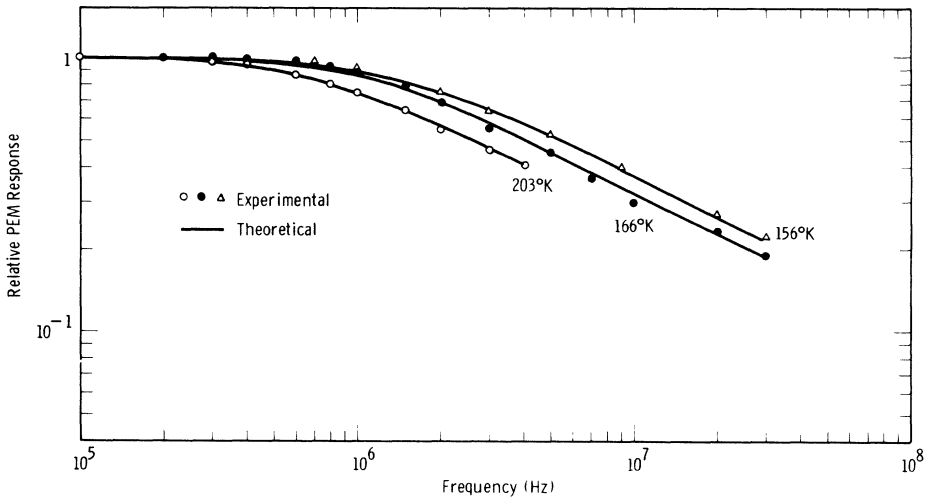

FIG. 9. Comparison between theoretical and experimental PEM frequency response for the p-type sample of Fig. 5 at 156, 165, and 203 °K. The theoretical curves were computed by using recombination parameter values given in Table I.

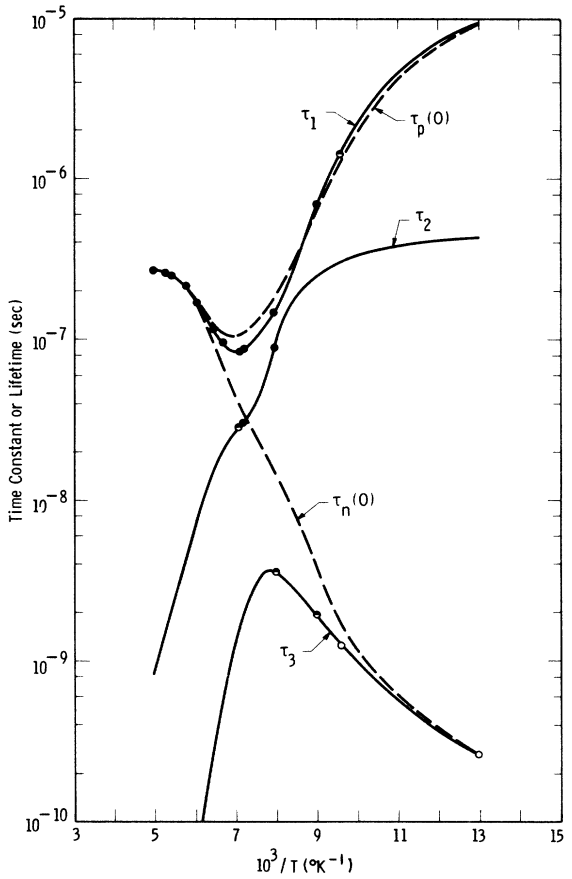

FIG. 10. Temperature dependence of the three time constants τ_1, τ_2, and τ_3 calculated from the recombination model given in Table I. The significance of the filled, half-filled, and unfilled circles is explained in the text.

temperature, because $H_2 \approx c_{p2}p$ and hence $H_2 \propto p$. On the other hand, at the high temperatures (> 150 °K) $H_2 \approx c_{n2}n$, and hence τ_2 decreases rapidly.

The temperature dependence of τ_2 at the intermediate temperatures arises mainly from p_2 in H_2, since over this temperature range $H_2 \approx c_{p2}(p+p_2)$. However, the presence of u_{n2} in Eq. (64) tends to slow down the decrease of τ_2 around 140 °K, and causes the slight knee to develop in this region.

3. *Time Constant* τ_3

The general behavior of τ_3 can be accounted for by the following simplified form of Eq. (49):

$$\tau_3^{-1} \approx H_1(1 + u_{n1} + u_{n2}) , \tag{65}$$

with further simplifications resulting in the following temperature ranges: from 77 to 111 °K, $\tau_3 \approx 1/H_1 u_{n1}$; from 111 to 150 °K, $\tau_3 \approx 1/H_1(u_{n1}+u_{n2})$; and from 150 °K upwards, $\tau_3 \approx 1/H_1$.

The temperature variation of τ_3 at temperatures below the peak in the τ_3 curve in Fig. 10 arises from u_{n1} and u_{n2}, both of which are decreasing functions of temperature. However, at temperatures beyond this, the variation is governed by the rapid decrease of H_1.

From the foregoing analysis of the three time constants, it may be inferred that the calculated PEM response curves are sensitive to (a) the choice of c_{p1} and $c_{n1}N_1$ at low temperatures where the theoretical response is dominated by the τ_1 and τ_3; (b) the choice of c_{p2} and $c_{n2}N_2$ at intermediate temperatures where the response is governed by τ_1 and τ_2; and (c) the choice of $c_{p2}N_2$ at high temperatures where only τ_1 is important.

There is a marginal effect due to u_{n1} on τ_1 and τ_2 at the intermediate temperatures. Since over this range, $H_1 \approx c_{n1}n$, and therefore $u_{n1} \approx N_1/n$, we see that the choice of N_1 affects the calculations, but only slightly.

D. Validity of Small-Signal Assumption

The validity of all our analysis rests, of course, on the small-signal assumption. A detailed investigation of the PEM and PC effects under steady-state conditions when this assumption no longer applies has been reported by Beattie and Cunningham[13] for a p-type sample at 80 °K. More recently, Choo[14] has pointed out that for a two-independent-level model such as the one used in the present work, the restriction on Δn depends on the properties of the recombination centers and can be much less severe than the condition suggested by Beattie and Cunningham, namely, $\Delta n \ll n$.

To check the small-signal assumption, measurements of the low-frequency PEM response as a function of relative light intensity were carried out at low temperatures for the p-type sample considered in Sec. V. The results, as given in Fig. 11, show that except for the case of 78 °K, the PEM response is linear within the range of light intensity used in our experiment, indicating that the small-signal assumption was justified. The departure from linearity around the operating point for 78 °K is, however, not serious, particularly since, as we have shown above, an exact determination of the PEM response time was precluded by the frequency limitations of our apparatus.

It is interesting to note that the increase in the linearity range with increasing temperature, as shown in Fig. 11, is consistent with the following linearization condition derived by Choo[14] for a two-independent-level model:

$$c_{p1}(p+p_1) \gg c_{n1}\Delta n .$$

This is so, because for our p-type sample and the value of 0.71 eV for E_1 that we used, both p and p_1 are increasing functions of temperature.

VI. SUMMARY AND CONCLUSIONS

The high-frequency response of the PEM effect

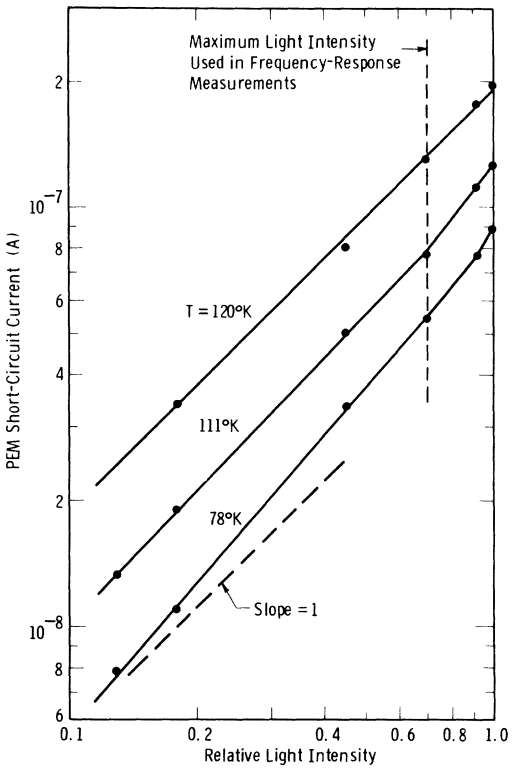

FIG. 11. Low-frequency PEM response to relative light intensity for the p-type sample of Fig. 5 at low temperatures. The magnetic-flux density used was 0.1 Wb/m^2.

in p-type InSb has been studied both theoretically and experimentally over the temperature range 77–203 °K. It was found that where the response curves could be characterized by a single time constant, the curves exhibited a high-frequency falloff with a 3-dB/octave slope, in contrast to the 6-dB/octave slope which was characteristic of the PC response. At temperatures around 200 °K, the same time constant entered into both the PEM and PC response. However, around 77 °K, the PEM time constant was at least some 3 orders of magnitude smaller than the PC time constant. This difference was shown theoretically to correspond to the difference between the steady-state electron and hole lifetimes, with which the PEM and PC time constants may, respectively, be identified.

The character of the PEM frequency-response curves was found to change as the temperature was increased from 77 to 203 °K, with evidence that more than one time constant was involved over the range 104–140 °K. All the response curves observed experimentally can be quantitatively accounted for in terms of a two-independent-level recombination model with parameters which are only slightly different from those used in previous work.

As a possible application, the findings at low temperatures suggest that, provided the practical problems of cooling the sample are resolved, conventional high-purity p-type InSb with its short minority-carrier lifetime could, when operated in the PEM mode, be very useful as a fast-response infrared detector, perhaps more so than the room-temperature detector element proposed by Zitter,[8] which would require additional doping to achieve the same response time. The room-temperature operation, coupled with the heavy doping, would reduce the resistivity of the detector, and this would have the adverse effect of decreasing the detectivity.[4]

ACKNOWLEDGMENTS

The authors gratefully acknowledge the advice and help of Dr. D. J. Roulston in solving the problems of instrumentation. This work was supported in part by the National Research Council of Canada.

APPENDIX: RATE-EQUATION MATRIX OF TWO-INDEPENDENT-LEVEL MODEL

The elements of the rate-equation matrix for the two-independent-level model have previously been given.[3] They are repeated below for easy reference:

$$
\begin{aligned}
&a_{11} = c_{n1}(n + n_1 + N_1^+) + c_{n2}N_2^+ , \quad a_{12} = -c_{n1}(n + n_1) , \\
&a_{13} = c_{n1}(n + n_1) - c_{n2}(n + n_2) , \quad a_{21} = -c_{p1}(p + p_1) , \\
&a_{22} = c_{p1}(p + p_1 + N_1^-) + c_{p2}N_2^- , \\
&a_{23} = -c_{p1}(p + p_1) + c_{p2}(p + p_2) , \\
&a_{31} = -c_{n2}N_2^+ , \quad a_{32} = c_{p2}N_2^- , \\
&a_{33} = c_{n2}(n + n_2) + c_{p2}(p + p_2) .
\end{aligned}
\tag{A1}
$$

*Present address: Westinghouse Research Laboratories, Pittsburgh, Pa. 15235.

[1]R. N. Zitter, A. S. Strauss, and A. E. Attard, Phys. Rev. 115, 266 (1959).

[2]R. A. Laff and H. Y. Fan, Phys. Rev. 121, 53 (1961).

[3]J. A. L. Hollis, S. C. Choo, and E. L. Heasell, J. Appl. Phys. 38, 1626 (1967).

[4]P. W. Kruse, in *Semiconductors and Semimetals*, edited by R. K. Willardson and A. C. Beer (Academic, New York, 1970), Vol. 5, p. 15.

[5]R. N. Zitter, Phys. Rev. 112, 852 (1958).

[6]W. Shockley, Bell System Tech. J. 28, 435 (1949).

[7]H. Fischer and P. von Thuena, Appl. Opt. 1, 373 (1962).

[8]R. N. Zitter, Rev. Sci. Instr. 35, 594 (1964).

[9]M. A. C. S. Brown, P. Porteous, and D. J. Solley, J. Sci. Instr. 44, 419 (1967).

[10]S. W. Kurnick and R. N. Zitter, J. Appl. Phys. 27, 278 (1956).

[11]Space-charge relaxation effects have been found to influence the noise spectra of high-resistivity semiconductors. See, for example, J. R. Fassett and K. M. van

Vliet, in *Proceedings of the International Conference of the Physics of Semiconductors, Exeter* (The Institute of Physics and The Physical Society, London, 1962), p. 886.
[12]S. C. Choo, Phys. Rev. B 1, 687 (1970).
[13]A. R. Beattie and R. W. Cunningham, Phys. Rev. 125, 533 (1962); J. Appl. Phys. 35, 353 (1964).
[14]S. C. Choo, Phys. Rev. B 3, 560 (1971).